JACS
JOURNAL OF THE AMERICAN CHEMICAL SOCIETY

Article

pubs.acs.org/JACS

Independent Ordering of Two Interpenetrating Magnetic Sublattices in the Double Perovskite Sr_2CoOsO_6

Ryan Morrow,[†] Rohan Mishra,[‡,⊥] Oscar D. Restrepo,[‡] Molly R. Ball,[‡] Wolfgang Windl,[‡] Sabine Wurmehl,[§,∥] Ulrike Stockert,[§,∥] Bernd Büchner,[§,∥] and Patrick M. Woodward*[,†]

[†]Department of Chemistry, The Ohio State University, Columbus, Ohio 43210-1185, United States

[‡]Department of Materials Science and Engineering, The Ohio State University, Columbus, Ohio 43210-1117, United States

[§]Leibniz Institute for Solid State and Materials Research Dresden IFW, D-01171 Dresden, Germany

[∥]Institute for Solid State physics, Technische Universität Dresden, D-01062 Dresden, Germany

Supporting Information

ABSTRACT: The insulating, fully ordered, double perovskite Sr_2CoOsO_6 undergoes two magnetic phase transitions. The Os(VI) ions order antiferromagnetically with a propagation vector $k = (1/2, 1/2, 0)$ below $T_{N1} = 108$ K, while the high-spin Co(II) ions order antiferromagnetically with a propagation vector $k = (1/2, 0, 1/2)$ below $T_{N2} = 70$ K. Ordering of the Os(VI) spins is accompanied by a structural distortion from tetragonal $I4/m$ symmetry to monoclinic $I2/m$ symmetry, which reduces the frustration of the face centered cubic lattice of Os(VI) ions. Density functional theory calculations show that the long-range Os−O−Co−O−Os and Co−O−Os−O−Co superexchange interactions are considerably stronger than the shorter Os−O−Co interactions. The poor energetic overlap between the 3d orbitals of Co and the 5d orbitals of Os appears to be responsible for this unusual inversion in the strength of short and long-range superexchange interactions.

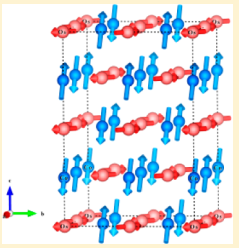

INTRODUCTION

Superexchange interactions govern cooperative magnetism in insulators. The strength of a given superexchange interaction depends upon the orbitals involved and generally decreases rapidly as the distance between the magnetic ions increases. The Goodenough−Kanamori rules[1,2] provide a simple, yet accurate, means of determining the sign of the superexchange interactions. These simple concepts are used by scientists to guide their search for new magnetic materials. In this article we report the crystal and magnetic structures of Sr_2CoOsO_6, a quaternary transition-metal oxide with the double perovskite structure. The $A_2MM'O_6$ double perovskites are among the most interesting classes of transition-metal oxides.[3] Compared to simpler AMO_3 ternary perovskites, the presence of chemical order of M and M′ cations profoundly impacts both the electronic structure and the magnetic coupling, in part because there are a greater variety of magnetic exchange interactions at work in the double perovskite structure. The results presented here show that long-range superexchange interactions between ions of the same type (i.e., Co−O−Os−O−Co and Os−O−Co−O−Os) are much stronger than the shorter nearest-neighbor Co−O−Os superexchange interactions. This result has broad implications for the way we think about magnetism in mixed 3d−5d transition-metal oxides.

The double perovskite structure, with general formula $A_2MM'O_6$, consists of a cubic, corner connected network of MO_6 and $M'O_6$ octahedra that alternate in all three directions, so that each MO_6 octahedron is connected only to $M'O_6$ octahedra and vice versa, as shown in Figure 1. An illustrative example is Sr_2CrOsO_6 where high-temperature ferrimagnetism

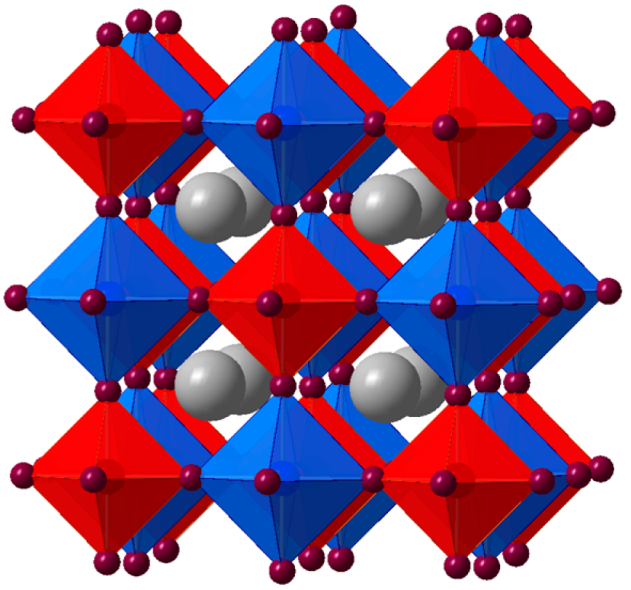

Figure 1. The $A_2MM'O_6$ double perovskite structure. The large A cations are shown in gray, while the M and M′ centered octahedra are shown in red and blue, respectively.

($T_C = 720$ K)[4] results from strong, antiferromagnetic Cr(III)−O−Os(V) superexchange coupling, as predicted by the Goodenough−Kanamori rules. According to those same rules

Received: July 17, 2013

   dx.doi.org/10.1021/ja407342w | J. Am. Chem. Soc. XXXX, XXX, XXX−XXX

adding electrons to the e_g orbitals of the 3d ion, for example, by replacing Cr with Fe(III), Co(II) or Ni(II), should change the sign of the superexchange interactions and stabilize an insulating ferromagnet with a high T_C—a rare combination.[5] To test this hypothesis as well as to better understand the rules that dictate 3d−5d superexchange we have prepared and characterized Sr_2CoOsO_6, a compound first prepared by Sleight et al.,[6] but whose magnetic and electrical properties were previously unknown.

EXPERIMENTAL SECTION

Batches of at most 1.6 g (3.075 mmol) Sr_2CoOsO_6 powder were prepared by a solid-state method utilizing stoichiometric quantities of SrO_2 (Sigma Aldrich, 98% pure), Co_3O_4 (Fischer Scientific, 99.8% pure), and Os metal (Alfa Aesar, 99.98% pure). The mixture was loaded into a capped alumina tube and placed in a quartz tube, of ∼40 mL volume with 3 mm thick walls, along with an additional capped alumina vessel containing PbO_2. The quartz tube was then evacuated and sealed prior to firing in a furnace to 1000 °C for 48 h within a fume hood. The PbO_2 was reduced to PbO at elevated temperatures, acting as an in situ source of oxygen gas to fully oxidize Os without allowing appreciable loss of volatile OsO_4.[7,8] The best results were obtained when the amount of PbO_2 was enough to produce an excess of one-quarter mole O_2 per mole of Sr_2CoOsO_6 produced. The reaction can be represented as follows:

$$12SrO_2 + 2Co_3O_4 + 6Os + (7PbO_2) \rightarrow 6Sr_2CoOsO_6 + (7PbO) + 3/2O_2$$

Phase purity and chemical ordering was established via XRD utilizing a Bruker D8 Advance Diffractometer equipped with a Cu source and an incident beam Ge(111) monochromator. Refinement indicated negligible loss of osmium. An X-ray powder diffraction pattern for this sample can be found in Figure S1.

Note that when heating osmium metal or binary osmium oxides it is important to confine the reactants to a sealed vessel and take precautions in case a leak of the vessel occurs, due to the formation of the highly toxic OsO_4(g) upon heating.

Variable-temperature neutron powder diffraction measurements were conducted on the POWGEN[9] beamline at Oak Ridge National Laboratory's Spallation Neutron Source. A sample size of ∼1.6 g contained within an 8 mm vanadium can was used for these experiments. Two wavelength ranges were measured at each temperature producing histograms with *d*-spacing ranges of 0.2760−3.0906 and 2.2076−10.3019 Å, referred to as Frames 1.5 and 5, respectively. Long scan times of 1 h for Frame 1.5 and 2 h for Frame 5 were collected at 12, 80, 130, and 300 K, while brief 5 min scans were collected in each frame at 10 K intervals.

The *k* vectors were determined by k search implemented in Fullprof,[10] symmetry analysis was performed and magnetic cells were generated utilizing SARAh,[11] and refinements were conducted with the Rietveld method as implemented in GSAS EXPGUI.[12,13] The magnetic form factor for osmium was input manually using the parameters given by Kobayashi et al.[14]

The magnetic susceptibility of Sr_2CoOsO_6 was collected within the temperature range of 5−400 K with both zero-field cooled and field cooled conditions under the effect of an applied field of 1 kG. These measurements were accomplished utilizing a Quantum Design MPMS SQUID magnetometer. A 46.6 mg sample was contained in a gelatin capsule and mounted in a straw for insertion into the instrument. No diamagnetic corrections for this sample holder were taken into account due to the large contribution of the sample.

Sr_2CoOsO_6 powder was pressed into a pellet prior to being sintered at 1100 °C and being cut into an approximate bar shape. The density was calculated to be 66.9% of the theoretical density of the material. Four-point contacts were secured to the pellet with silver paint before dc electrical measurements of the sample were conducted within the temperature range 5−350 K utilizing a Quantum Design Physical Property Measurement System (PPMS). Below 47 K the resistance of the sample became too high to measure accurately.

Specific heat capacity was measured with a PPMS, Quantum Design, using a relaxation method. Sr_2CoOsO_6 was measured in zero magnetic field between 2 and 298 K using small, disc-like samples of roughly 11 mg. In order to thermally couple the sample to the calorimeter, Apiezon grease was used. The specific heat of the Apiezon grease was measured alone, first over the whole temperature range and then subtracted from the total value of the subsequent measurement which included the sample, to derive the specific heat contribution from the sample only.

Density functional theory (DFT) calculations were performed using the Vienna ab initio Simulation Package (VASP).[15,16] The influence of the core electrons was incorporated using projector augmented wave (PAW) potentials[17] within the spin-polarized generalized gradient approximation (GGA) exchange−correlation functional.[18] The plane-wave cutoff energy was set at 525 eV. The Brillouin zone was sampled using dense Monkhorst−Pack *k*-point meshes,[19] with mesh divisions N_i such that the product of N_i with the corresponding lattice vectors was as close as possible to 50 Å. The low-temperature (12 K) experimental lattice constants and ionic coordinates obtained from neutron diffraction studies were used in the calculations without performing any structural or ionic relaxations. The collinear magnetic calculations were performed on 20 to 160 atoms supercells. The experimentally observed magnetic structure was studied using a 160 atom cell, and noncollinear calculations were performed by including spin−orbit interactions as implemented in VASP.[20]

To include the strong correlations in the transition-metal elements, we have used the rotationally invariant Dudarev approach[21] to GGA +*U*,[22] in which only one effective Hubbard parameter U_{eff} is used. Given that U_{eff} is not precisely determined by experiment or theory, we have examined a range of U_{eff} values: 0 and 4.1 eV for Co and 0, 2.1, and 4.1 eV for Os. While the order of stability of different magnetic configurations remains the same for all combinations of U_{Co} and U_{Os}, we find that U_{Co} = 4.1 eV and U_{Os} = 2.1 eV also reproduce the experimentally observed insulating nature. Hence, we use this particular combination of U_{Co} and U_{Os} to determine the exchange energies.

RESULTS AND DISCUSSION

The magnetic susceptibility of Sr_2CoOsO_6 as a function of temperature is shown in Figure 2. As signaled by the cusps in the data, Sr_2CoOsO_6 appears to undergo two antiferromagnetic transitions at temperatures of approximately T_{N1} = 108 K and T_{N2} = 70 K. The inverse susceptibility in the paramagnetic regime 200−400 K follows the Curie−Weiss law. The Weiss temperature, θ, extracted from the Curie−Weiss fit was found

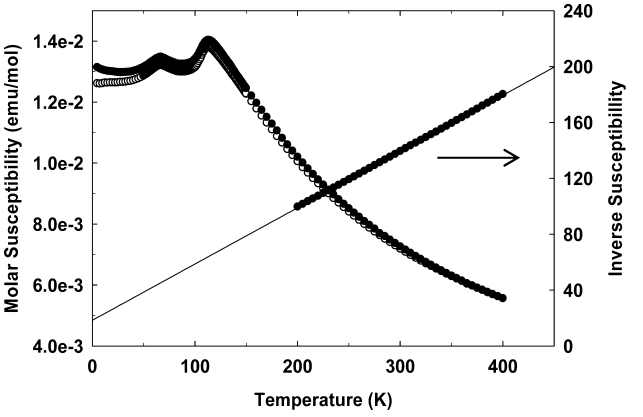

Figure 2. Field cooled (filled circles) and zero field cooled (open circles) magnetic susceptibility with inverse zero field cooled data plotted against the right axis showing the linear Curie−Weiss fit.

dx.doi.org/10.1021/ja407342w | J. Am. Chem. Soc. XXXX, XXX, XXX−XXX

to be −51 K. The atypical observation that θ is lower than either of the Neél temperatures suggests the presence of ferromagnetic interactions that compete with the antiferromagnetic interactions. As we will see later DFT calculations confirm the presence of competing ferromagnetic and antiferromagnetic superexchange interactions. The effective magnetic moment per formula unit obtained from the Curie–Weiss fit is μ_{eff} = 4.46 μ_B, which is in reasonably good agreement with the expected spin-only value calculated assuming the presence of Os(VI) and high-spin (HS) Co(II), $\mu_{spin} = [\mu_{spin}(Co)^2 + \mu_{spin}(Os)^2]^{1/2}$ = 4.80 μ_B. However, it should be noted that HS Co(II) has been reported in related double perovskites to have an effective moment which is higher than the spin-only value of 3.87 μ_B due to a constructive contribution from unquenched orbital moment,[23−26] and the orbital contribution if present for Os(VI) would tend to reduce the moment of that ion from its spin-only value of 2.83 μ_B.[27] Thus it is quite plausible that orbital angular momentum contributes to the moment of both ions, but the effects average out to give an overall μ_{eff} close to the spin-only value.

Specific heat measurements on Sr_2CoOsO_6 reveal two pronounced anomalies on cooling, at 108 and 70 K (Figure 3). These temperatures correspond closely to the cusps seen in

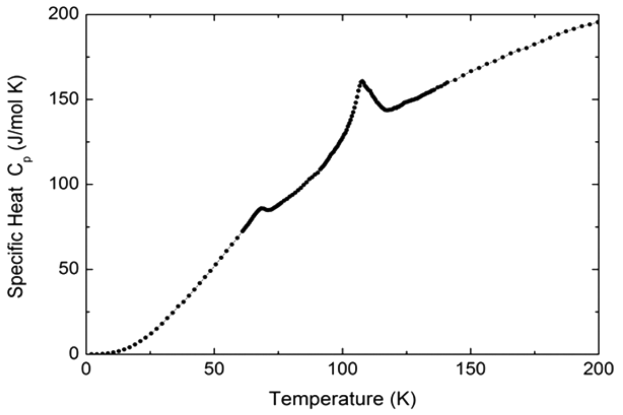

Figure 3. Specific heat of Sr_2CoOsO_6 as a function of temperature.

the magnetic susceptibility measurements. The 70 K transition peak has a λ-shape, normally seen for a second-order phase transition. This observation, taken together with the susceptibility measurements, suggests a purely magnetic phase transition. On the other hand, the rather symmetric shape of the peak at 108 K suggests a first-order phase transition, which would be expected if a structural phase transition accompanies the magnetic transition, as confirmed by the diffraction measurements discussed below.

Electrical transport measurements reveal insulating behavior as resistivity rises rapidly with decreasing temperature, as shown in Figure 4. The log of the conductivity shows a linear $T^{-1/4}$ temperature dependence (see Supporting Information) which is consistent with variable range hopping transport, whereby electrons hop between localized states. There is a continuous deviation which occurs between the phase transitions, leading to two separate linear fits above and below the transitions. The mathematical form of variable range hopping conductivity is given as $\sigma = \sigma_0 e^{(-A/T^{1/4})}$. The fitted A factors found above and below this transition temperature are 43.12(2) and 46.14(9), respectively.

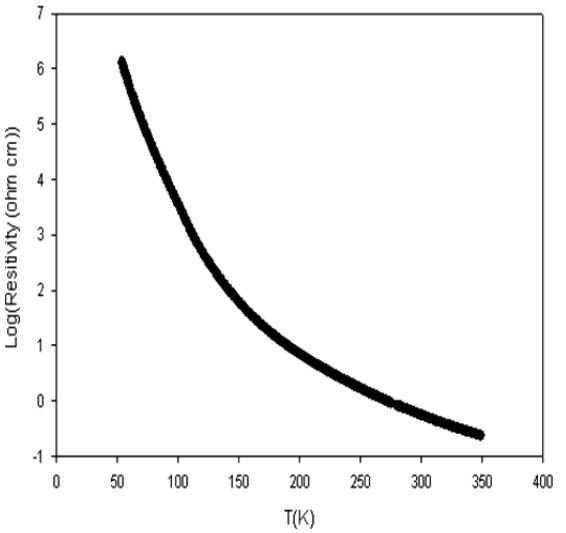

Figure 4. Log resistivity vs temperature.

Variable-temperature time-of-flight neutron powder diffraction measurements were collected to obtain accurate structural parameters and to probe the magnetic structure. At room temperature both X-ray and neutron powder diffraction patterns can be fit to a tetragonally distorted, ordered double perovskite structure with $I4/m$ symmetry and complete ordering of Co and Os. The tetragonal distortion occurs due to rotations of the octahedra about the c-axis ($a^0a^0c^-$ tilting)[3] and a relatively subtle axial elongation of the octahedra. This relatively common distortion of the structure is also observed at room temperature in double perovskites such as Sr_2NiOsO_6,[7] Sr_2FeMoO_6,[28] and Sr_2CoReO_6.[22] The evolution of the structure was studied with variable-temperature neutron powder diffraction, and the results are shown in Figure 5. On cooling below 108 K, where magnetic ordering sets in, an abrupt structural distortion occurs lowering the symmetry to the monoclinic space group $I2/m$. The splitting of the (220) reflection signaling the transition from tetragonal to monoclinic symmetry is shown in Figure S3.

The Co–O and Os–O distances are plotted as a function of temperature in Figure 5. In the high-temperature tetragonal structure the axial Co–O(1) and Os–O(1) bonds are slightly longer than the Co–O(2) and Os–O(2) bonds that lie in the xy-plane. This type of distortion could be associated with a Jahn–Teller distortion arising from the orbital degeneracy of either the HS d^7 Co(II) ion or the d^2 Os(VI) ion. The magnitude of the distortion is relatively small, but this is not unexpected for a Jahn–Teller distortion arising from partial occupation of the t_{2g} orbitals.

In both the tetragonal and monoclinic phases the bond lengths are consistent with the assignment of HS Co(II) and Os(VI) oxidation states,[29,30] so we can rule out a change in spin-state or some type of Co–Os charge transfer as the driving force behind the transition. Furthermore, the $a^0a^0c^-$ pattern of octahedral tilting is maintained, so we can also rule out octahedral tilting as the driving force for the phase transition. Instead the transition appears to be most closely linked to distortions of the CoO_6 octahedra, as shown in Figure 5.

In the low-temperature monoclinic structure the symmetry is lowered in such a way that there are three unique bond distances within each octahedron. Despite the reduction in symmetry, the two long/four short distortion of the osmium

dx.doi.org/10.1021/ja407342w | J. Am. Chem. Soc. XXXX, XXX, XXX–XXX

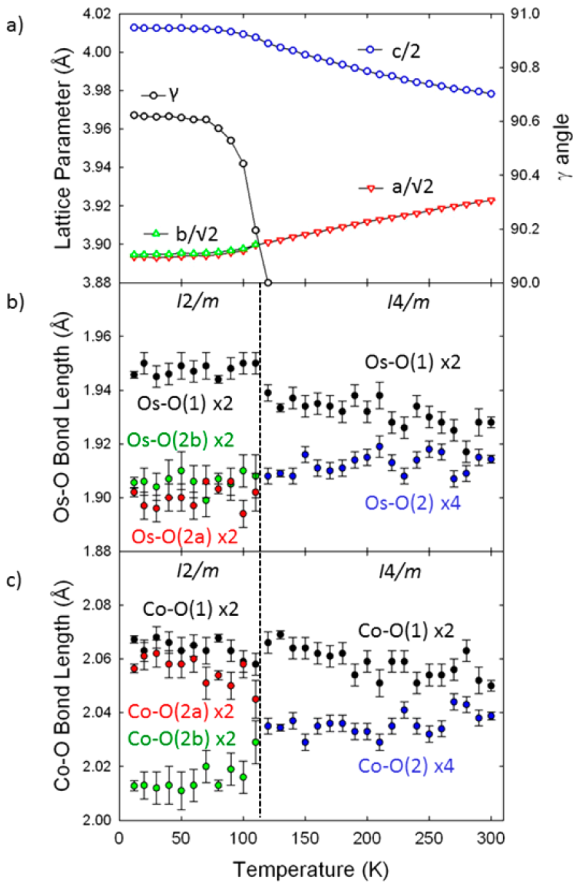

Figure 5. Evolution of the (a) lattice parameters and (b) Os−O and (c) Co−O bond lengths as a function of temperature, as extracted from variable-temperature neutron diffraction data. The dashed line separates the tetragonal *I*4/*m* phase from the monoclinic *I*2/*m* phase.

Table 1. Lattice Parameters, Quality of Fit, and Atomic Moments Resulting from Rietveld Refinement of Neutron Powder Diffraction Data

	12 K	80 K	130 K	300 K
space group	*I*112/*m*	*I*112/*m*	*I*4/*m*	*I*4/*m*
a (Å)	5.5061(1)	5.5079(1)	5.51867(7)	5.54786(8)
b (Å)	5.5079(1)	5.5097(1)	–	–
c (Å)	8.0258(1)	8.0235(1)	8.0049(1)	7.9565(1)
V (Å)^3	243.386(3)	243.48(1)	243.796(9)	244.891(9)
γ (°)	90.623(1)	90.574(1)	–	–
χ^2	3.38	3.27	3.89	3.86
R_{wp}	1.88	1.86	2.03	2.02
R_p	3.02	2.9	3.06	3.05
Os moment	1.81(4) μ_B	1.57(5) μ_B	–	–
Co moment	2.90(5) μ_B	–	–	–

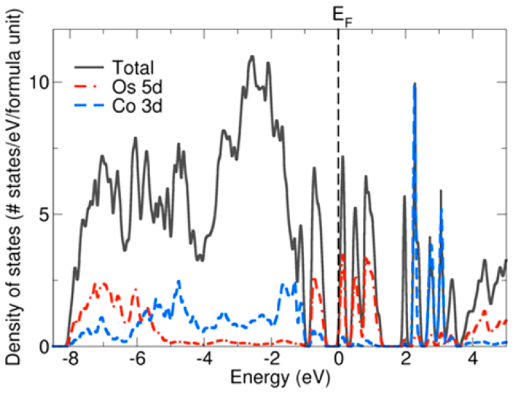

Figure 6. Total- and atom-resolved density of states of Sr_2CoOsO_6 from a noncollinear DFT calculation with U_{Co} = 4.1 eV and U_{Os} = 2.1 eV. The contributions of the Os 5d and Co 3d orbitals are shown in red and blue, respectively.

octahedron is essentially retained with bond distances of 2 × 1.946(1) Å, 2 × 1.902(2) Å, and 2 × 1.906(2) Å. In contrast the distortion of the cobalt octahedron changes at the phase transition, and this change is responsible for lowering the symmetry to monoclinic. In the tetragonal structure all four of the equatorial Co−O(2) bonds are the same length, 2.036(1) Å at 130 K. This square base distorts in the monoclinic structure to give two bonds of 2.013(2) Å and two bonds of 2.056(2) Å. The longer of these two sets of bonds is comparable to the axial Co−O(1) distance, 2.067(1) Å, so that the octahedron now has four long and two short bonds. This type of distortion is unusual for Co(II). A thorough literature search revealed only one other Co^{2+}-containing perovskite with a similar distortion, La_2CoIrO_6.[31]

Table 1 gives information concerning the unit cell and goodness of fit parameters for each refinement on the longer neutron data sets. Figures and tables containing further details on the structure of Sr_2CoOsO_6 at different temperatures can be found in the Supporting Information.

Figure 6 shows the electronic density of states calculated using DFT. The 5d t_{2g} orbitals of osmium make the major contribution at the Fermi level, but correlations open up a small gap in what would otherwise be a one-third filled band. The prediction of insulating behavior is consistent with our resistivity measurements.

Upon cooling below T_{N1} = 108 K, an additional set of reflections arise in the neutron diffraction pattern that cannot be attributed to the structural phase transition, one such reflection is found at *d* = 7.7 Å as shown in Figure 7. These reflections signal the onset of antiferromagnetic order and can be accounted for with a magnetic propagation vector *k* = 1/2, 1/2, 0. Two irreducible representations are consistent with this propagation vector and *I*2/*m* symmetry, but only the Γ(3)

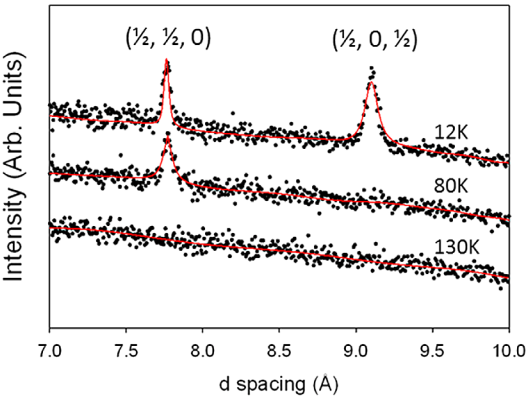

Figure 7. Rietveld fits to the high *d*-spacing regions of the neutron diffraction patterns showing the presence/absence of magnetic reflections at three temperatures: above T_{N1} (130 K), between T_{N1} and T_{N2} (80 K), and below T_{N2} (12 K). Black symbols represent observed data, while the red curves represent the calculated patterns. The *hkl* values given in the figure are indexed on the nuclear cell.

dx.doi.org/10.1021/ja407342w | J. Am. Chem. Soc. XXXX, XXX, XXX−XXX

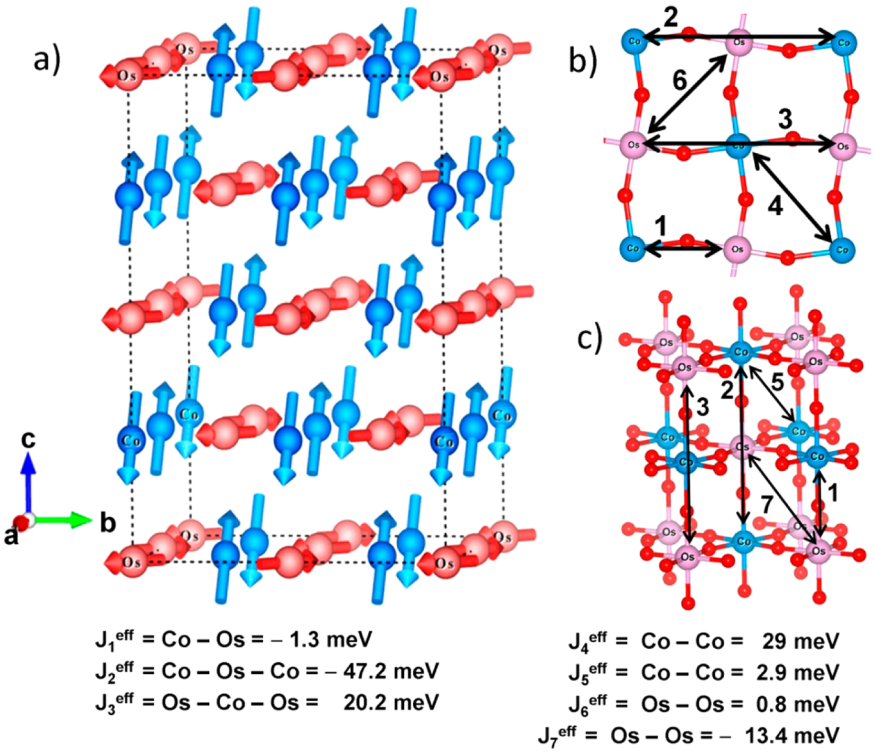

Figure 8. (a) Experimentally determined magnetic structure of Sr_2CoOsO_6, with the Os shown in red and the Co in blue. (b) A schematic of the superexchange pathways between Co and Os ions with the exchange constants extracted from the DFT calculations. A positive (negative) value of J indicates ferromagnetic (antiferromagnetic) coupling.

representation, with basis vectors in the a and b directions, is able to correctly reproduce the observed intensities of the magnetic reflections. Refinements of a long data set collected at 80 K yield a moment of 1.57(5) μ_B if one assumes ordering of Os(IV), or 1.68(5) μ_B if one assumes ordering of Co(II). It was also possible to fit the data reasonably well with non-negligible moments on both Co and Os by fixing the moment on one atom to an intermediate value, such as 0.8 μ_B, and refining the moment on the other. However, those refinements always gave slightly higher R_{wp} values and poorly fit one of the magnetic reflections. This observation lends support to the hypothesis that between 70−110 K only one magnetic sublattice orders.

On cooling below T_{N2} a second set of magnetic reflections emerge that can be indexed with a propagation vector k = 1/2, 0, 1/2, the strongest of which is the peak at d = 9.1 Å seen in Figure 7. Due to the similarity of the a and b lattice parameters, it is possible to produce a nearly identical quality solution using a propagation vector of vector k = 0, 1/2, 1/2, due to powder averaging. The following analysis and conclusions are not affected by this choice of propagation vector. A symmetry analysis yields only one irreducible representation, Γ(2), for this second set of magnetic peaks. Although the Γ(2) representation has three basis vectors, only the two oriented in the a and c directions were needed to model the intensities of the magnetic reflections. It should also be noted that the emergence of a second set of magnetic reflections below T_{N2} does not lead to any noticeable change in the intensities of the first set of magnetic reflections. A low-temperature magnetic structure model was derived by combining the k = 1/2, 1/2, 0 ordering scheme on one magnetic sublattice, and the k = 1/2, 0, 1/2 scheme on the other sublattice, leading to a 2 × 2 × 2 magnetic unit cell, shown in Figure 8a. In this structure the cobalt and osmium spins are noncollinear, with both sublattices adopting antiferromagnetic order.

While the neutron diffraction experiments provide strong support for independent ordering of cobalt and osmium ions, it is not immediately apparent which ion orders at the higher temperature. If we assume that the cobalt ions order at 108 K and the osmium ions order at 70 K, refinements of the 12 K data set yield atomic moments of 1.99(4) μ_B and 2.71(4) μ_B for these two ions, respectively. These values are not physically reasonable because a moment of 2.71 μ_B for the d^2 Os(VI) ion is larger than the spin-only value of 2 μ_B, and any orbital contribution would be expected to reduce, not increase, the moment. Using the opposite assumption, osmium ordering at 108 K and cobalt ordering at 70 K, gives moments of 1.81(4) μ_B and 2.90(5) μ_B that are quite close to the high field, spin-only values of 2 μ_B and 3 μ_B expected for the Os(VI) and HS d^7 Co(II) ions, respectively. DFT calculations give moments of 1.69 μ_B and 2.71 μ_B for osmium and cobalt, respectively. These values are in close agreement with the experimentally obtained values, and the agreement strongly supports the conclusion that the osmium ions order at 108 K and the cobalt ions at 70 K.

The neutron refinements reveal a complex magnetic structure, but they do not provide direct information as to why this magnetic structure is more stable than simpler alternatives normally seen in perovskites. DFT calculations were performed in order to extract the magnetic coupling constants that are responsible for the unusual magnetism observed in this compound.[32] There is one prior report of DFT calculations on Sr_2CoOsO_6, but in that study they only looked at the ferromagnetic and ferrimagnetic configurations, concluding that Sr_2CoOsO_6 should be a ferrimagnetic half-metal.[33] However, as shown here the actual ground state is an

dx.doi.org/10.1021/ja407342w | J. Am. Chem. Soc. XXXX, XXX, XXX−XXX

antiferromagnetic insulator, which lessens the validity of the conclusions made in the earlier computational study.

The relative energies of 10 magnetic configurations were calculated, and the experimentally observed noncollinear, antiferromagnetic ground state with a 2 × 2 × 2 unit cell was found to be the lowest-energy configuration (see Supporting Information). The ferromagnetic configuration was 809 meV per f.u. higher in energy, while the ferrimagnetic configuration was 776 meV higher in energy. The exchange constants, for seven exchange pathways of potential importance were extracted from these calculations and are given in Figure 8. To minimize correlations in the fitting procedure the through bond superexchange constants J_1^{eff}, J_2^{eff}, and J_3^{eff} were constrained to be the same in all three directions. Because the direct exchange coupling between ions of the same type across a face of the unit cell can be quite sensitive to octahedral tilting, we have used two different J values for Co−Co coupling, J_4^{eff} and J_5^{eff}, and two for Os−Os coupling, J_6^{eff} and J_7^{eff}.

The calculations reveal very weak coupling, $J_1^{eff} = -1.3$ meV for the nearest-neighbor Co−O−Os superexchange pathways that are the shortest interactions and would normally be expected to be the strongest. The largest superexchange coupling is found for the four bond Co(↑)−O−Os−O−Co(↓) interaction, which is antiferromagnetic with $J_2^{eff} = -47.2$ meV. The four bond Os(↑)−O−Co−O−Os(↑) interaction is also quite strong, with $J_3^{eff} = 20.2$ meV, but ferromagnetic. The in-plane Co−Co coupling, J_4^{eff} was also relatively strong, 29 meV, but this value was somewhat dependent on the constraints used with fitting J values to the calculated energies of the various magnetic structures.

To our knowledge it is unprecedented that these long superexchange pathways could emerge as being much stronger than the shorter nearest-neighbor interactions along the same path, but a closer look at the experimental structure shows that all Os−O−Co−O−Os interactions are indeed ferromagnetic, while all of the Co−O−Os−O−Co interactions are antiferromagnetic. Examination of the partial density of states of the Co and Os ions (Figure 6) shows that there is only a small overlap of the Co 3d and Os 5d states (particularly for the e_g orbitals), which helps to explain the weak nearest-neighbor interaction between the two ions. In other words the poor energetic overlap of the Co 3d and Os 5d orbitals (once hybridized with oxygen) leaves the two sublattices relatively uncoupled.

Before finishing let us return to the unusual four long/two short distortion of the cobalt octahedron that occurs on cooling below T_{N1}. While there is no way to rationalize this type of distortion based solely on the electron configuration of the HS Co(II) ions, the fact that the distortion accompanies ordering of the osmium spins provides an important clue. In the double perovskite structure the osmium ions sit on a face centered cubic (fcc) lattice, which is a geometrically frustrated lattice. While all Os−O−Co−O−Os superexchange interactions are ferromagnetic, there are four independent but interpenetrating sublattices of Os ions that do not interact with each other via this exchange route. These sublattices interact through nearest-neighbor Os−Os exchange given as J_6 nd J_7 in Figure 8. In the high-temperature tetragonal structure, the Os−Os nearest-neighbor distances are 5.51 Å (× 4) and 5.59 Å (× 8). This arrangement is slightly distorted from a perfect fcc lattice but still highly frustrated. In the low-temperature monoclinic structure the distances become 5.51 Å (× 4), 5.57 Å (× 4), and 5.61 Å (× 4). These distances represent the nearest-neighbor distances from one Os sublattice to the other three independent Os sublattices. The two sublattices that are aligned ferromagnetically with each other are separated by the longest of these three distances, 5.61 Å. Thus the structural distortion that accompanies T_{N2} reduces the frustration of the fcc arrangement of osmium ions by shortening the Os−Os distances between the eight nearest-neighbor antiferromagnetically coupled Os ions and increasing the distances between the four nearest-neighbor ferromagnetically coupled Os ions. Based on this observation we hypothesize that the structural transition at 108 K, and the resulting unusual distortion of the CoO_6 octahedron, is driven by magnetic ordering of the Os spins.

CONCLUSIONS

The double perovskite Sr_2CoOsO_6 undergoes two magnetic phase transitions on cooling from room temperature. The two interpenetrating sublattices of Os(VI) and Co(II) each order antiferromagnetically but independent of each other. The Os(VI) spins order antiferromagnetically below 108 K, while the Co(II) spins order antiferromagnetically below 70 K. The observed magnetic structure suggests and the computational results confirm that four bond superexchange interactions, Os−O−Co−O−Os and Co−O−Os−O−Co, are stronger than the nearest-neighbor Os−O−Co superexchange interactions. This highlights a fundamental difference between double perovskites containing 3d and 5d ions, with more familiar perovskites containing only 3d ions. These results provide a fascinating glimpse of superexchange coupling in mixed 3d−5d transition-metal oxides, revealing a complexity that was not previously appreciated. Further studies on a variety of $A_2MM'O_6$ double perovskites with varying electron count, orbital energies, and structural distortions are needed to better understand the factors that control the strength and sign of superexchange coupling in mixed 3d−5d transition-metal oxides. Furthermore, the presence of competing long-range antiferromagnetic and ferromagnetic exchange interactions provides a route to materials where dramatic changes in properties can result in response to relatively subtle changes in structure.

ASSOCIATED CONTENT

Supporting Information

Refined XRD and NPD diffraction patterns; refinement details; crystal structure representation; electronic transport fit details; DFT calculation details. This information is available free of charge via the Internet at http://pubs.acs.org.

AUTHOR INFORMATION

Corresponding Author

woodward@chemistry.ohio-state.edu

Present Address

[⊥]Department of Physics and Astronomy, Vanderbilt University, Nashville, Tennessee 37235, United States

Notes

The authors declare no competing financial interest.

ACKNOWLEDGMENTS

Support for this research was provided by a Materials World Network Grant funded by the National Science Foundation (award no. DMR-1107637) and the DFG (project WU595/5-1). Partial support was supplied by the Center for Emergent Materials an NSF Materials Research Science and Engineering Center (DMR-0820414). A portion of this research was carried

out at Oak Ridge National Laboratory's Spallation Neutron Source, which is sponsored by the U.S. Department of Energy, Office of Basic Energy Sciences. S.W. acknowledges funding by Deutsche Forschungsgemeinschaft DFG under the Emmy-Noether programme (project WU595/3-1). DFT calculations were performed at the Ohio Supercomputer Center (grant no. PAS0072). The authors thank Ashfia Huq for assistance with the neutron diffraction experiments. John Goodenough, Art Sleight, and Warren Pickett are acknowledged for helpful suggestions and comments as well as Konstantin Nenkov, Steven Rodan, and Mahmoud Abdel-Hafiez for technical support.

REFERENCES

(1) Goodenough, J. B. *Phys. Rev.* **1955**, *100*, 564−573.
(2) Kanamori, J. *J. Phys. Chem. Solids* **1959**, *10*, 87−98.
(3) Lufaso, M. W.; Barnes, P. W.; Woodward, P. M. *Acta Cryst. B* **2006**, *62*, 397−410.
(4) Krockenberger, Y.; Mogare, K.; Reehuis, M.; Tovar, M.; Jansen, M.; Vaitheeswaran, G.; Kanchana, V.; Bultmark, F.; Delin, A.; Wilhelm, F.; Rogalev, A.; Winkler, A.; Alff, L. *Phys. Rev. B* **2007**, *75*, 020404(R).
(5) Rogado, N. S.; Li, J.; Sleight, A. W.; Subramanian, M. A. *Adv. Mater.* **2005**, *17* (18), 2225−2227.
(6) Sleight, A. W.; Longo, J.; Ward, R. *Inorg. Chem.* **1962**, *1* (2), 245−250.
(7) Macquart, R.; Kim, S. J.; Gemmill, W. R.; Stalick, J. K.; Lee, Y.; Vogt, T.; Zur Loye, H. C . *Inorg. Chem.* **2005**, *44*, 9676−9683.
(8) Lufaso, M. W.; Gemmill, W. R.; Mugavero, S. J.; Kim, S. J.; Lee, Y.; Vogt, T.; zur Loye, H. C. *J. Solid State Chem.* **2008**, *181* (3), 623−627.
(9) Huq, A.; Hodges, J. P.; Gourdon, O.; Heroux, L. *Z. Kristallogr. Proc.* **2011**, *1*, 127−135.
(10) Rodriguez-Carvajal, J. *Physica B* **1993**, *192*, 55−69.
(11) Wills, A. *Physica B* **1991**, *276*, 680−681.
(12) Larson, A. C.; Von Dreele, R. B. *Los Alamos National Laboratory Report LAUR*; Los Alamos National Laboratory: Los Alamos, NM, 2000; pp86−748 .
(13) Toby, B. H. *J. Appl. Crystallogr.* **1991**, *34*, 210−213.
(14) Kobayashi, K.; Nagao, T.; Ito, M. *Acta Crys. A* **1991**, *67*, 473−480.
(15) Kresse, G.; Hafner, J. *Phys. Rev. B* **1991**, *47*, 558−561.
(16) Kresse, G.; Hafner, J. *Phys. Rev. B* **1991**, *49*, 14251−14269.
(17) Blöchl, P. E. *Phys. Rev. B* **1991**, *50*, 17953−17979.
(18) Wang, Y.; Perdew, J. P. *Phys. Rev. B* **1991**, *44*, 13298−13307.
(19) Monkhorst, H. J.; Pack, J. D. *Phys. Rev. B* **1991**, *13*, 5188−5192.
(20) Hobbs, D.; Kresse, G.; Hafner, J. *Phys. Rev. B* **1991**, *62*, 11556−11570.
(21) Dudarev, S. L.; Botton, G. A.; Savrasov, S. Y.; Humphreys, C. J.; Sutton, A. J. *Phys. Rev. B* **1991**, *57*, 1505−1509.
(22) Anisimov, V. I.; Zaanen, J.; Andersen, O. K. *Phys. Rev. B* **1991**, *44*, 943−954.
(23) Viola, M. C; Martinez-Lope, M. J.; Alonso, J. A.; De Paoli, J. M.; Pagola, S.; Pedregosa, J. C.; Fernandez-Diaz, M. T.; Carbonio, R. E. *Chem. Mater.* **2003**, *15*, 1655−1663.
(24) Ivanov, S. A.; Eriksson, S. G.; Tellgren, R.; Rundlöf, H.; Tseggai, M. *Mater. Res. Bull.* **2005**, *40*, 840−849.
(25) Lopez, C. A.; Saleta, M. E.; Curiale, J.; Sanchez, R. D. *Mater. Res. Bull.* **2012**, *47*, 1158−1163.
(26) Retuerto, M.; Martínez-Lope, M. J.; García-Hernández, M.; Fernández-Díaz, M. T.; Alonso, J. A. *Eur. J. Inorg. Chem.* **2008**, *4*, 588−595.
(27) Choy, J. H.; Kim, D. K.; Kim, J. Y. *Solid State Ionics* **1998**, *108*, 159−163.
(28) Chmaissem, O.; Kruk, R.; Dabrowski, B.; Brown, D. E.; Xiong, X.; Kolesnik, S.; Jorgensen, J. D.; Kimball, C. W. *Phys. Rev. B* **2000**, *62*, 14197−14206.
(29) Shannon, R. D. *Acta Cryst. A* **1976**, *32*, 751−767.
(30) Brese, N. E.; O'Keefe, M. *Acta Cryst. B* **1991**, *47*, 192−197.
(31) Currie, R. C.; Vente, J. F.; Frikkee, E.; IJdo, D. J. W. *J. Solid State Chem.* **1995**, *116* (1), 199−204.
(32) Tian, C.; Wibowo, A. C.; Zur Loye, H.-C.; Whangbo, M.-H. *Inorg. Chem.* **2011**, *50*, 4142−4148.
(33) Wang, J.; Meng, J.; Wu, Z. *Chem. Phys. Lett.* **2011**, *501*, 324−329.